

RESEARCH ARTICLE



Engineered pulmonary artery tissues for measuring contractility, drug testing and disease modelling

Adam L. Fellows^{1,2} | Kate Quigley¹ | Venus Leung¹ | Alexander J. Ainscough¹ | Martin R. Wilkins¹ | Harry Barnett² | David Miller² | Manuel Mayr¹ | Beata Wojciak-Stothard¹

¹National Heart & Lung Institute, Imperial College London, London, UK

²Imperial College Advanced Hackspace, Imperial College London, London, UK

Correspondence

Adam L. Fellows, Department of Comparative Biomedical Sciences, Royal Veterinary College, London, UK.

Email: afellows@rvc.ac.uk

Funding information

Imperial British Heart Foundation Centre of Research Excellence; NHLI Foundation Pilot Award

Abstract

Background and Purpose: Vasoreactivity of pulmonary arteries regulates blood flow through the lungs. Excessive constriction of these vessels contributes to pulmonary arterial hypertension (PAH), a progressive and incurable condition, resulting in right heart failure. The search for new and improved drug treatments is hampered by laboratory models that do not reproduce the vasoactive behaviour of healthy and diseased human arteries.

Experimental Approach: We have developed an innovative technique for producing miniature, three-dimensional arterial structures that allow proxy evaluation of human pulmonary artery contractility. These “engineered pulmonary artery tissues” or “EPATs” are fabricated by suspending human pulmonary artery vascular smooth muscle cells (VSMCs) in fibrin hydrogels between pairs of silicone posts, located on custom-made racks, in 24-well culture plates.

Key Results: EPATs exhibit rapid, robust and reproducible contraction responses to vasoconstrictors (KCl, ET-1, U46619) as well as relaxation responses to clinically approved PAH vasodilatory drugs that target several signalling pathways, such as bosentan, epoprostenol, selexipag and imatinib. EPATs composed of pulmonary artery VSMCs from PAH patients exhibit enhanced contraction to vasoconstrictors and relaxation in response to vasodilators. We also demonstrate the incorporation of endothelial cells into EPATs for the measurement of endothelium-dependent dilatory responses.

Conclusion and Implications: We demonstrate the capacity and suitability of EPATs for studying the contractile behaviour of human arterial cells and preclinical drug testing. This novel biomimetic platform has the potential to dramatically improve our understanding and treatment of cardiovascular disease.

KEYWORDS

bioengineering, disease modelling, drug testing platform, pulmonary hypertension, vascular pharmacology

Abbreviations: ADMA, asymmetric dimethylarginine; EPAT, engineered pulmonary artery tissue; ET-1, endothelin-1; HPAEC, human pulmonary artery endothelial cell; PAH, pulmonary arterial hypertension; PASMC, pulmonary artery smooth muscle cell; PDMS, polydimethylsiloxane; U46619, 11 α ,9 α -epoxymethano-PGH₂.

This is an open access article under the terms of the [Creative Commons Attribution](https://creativecommons.org/licenses/by/4.0/) License, which permits use, distribution and reproduction in any medium, provided the original work is properly cited.

© 2025 The Author(s). *British Journal of Pharmacology* published by John Wiley & Sons Ltd on behalf of British Pharmacological Society.

1 | INTRODUCTION

Excessive vasoconstriction of the pulmonary arteries (Cahill et al., 2012) is the primary target of current therapies for pulmonary arterial hypertension (PAH) (Humbert, Sitbon, et al., 2023). A major hindrance to the development of new and better therapies for PAH has been the lack of appropriate preclinical models that capture the full phenotype of the human disease (Stenmark et al., 2009). This hindrance, combined with a lack of an accurate platform to measure human vasoreactivity *in vitro*, has limited our capacity to evaluate potential therapies, further widening the translational gap between bench and bedside.

Arterial control of blood flow is ultimately determined by the contractile state of vascular smooth muscle cells (VSMCs) within the medial layer of the vessel wall, wherein VSMC contraction leads to vasoconstriction and VSMC relaxation leads to vasodilation. Predictive measurements of human VSMC contractility in the laboratory are crucial to improving our understanding of vascular physiology and disease. Myography, the current gold standard technique, is performed *ex vivo* and, despite providing absolute measurements of force generation, suffers from being technically challenging, labour intensive, expensive and low throughput (Wenceslau et al., 2021). Myography also requires specialist equipment and access to fresh tissue, meaning that experiments are usually conducted in animals because access to healthy human vessels is severely limited. This limitation diminishes the translatability of findings because VSMC contractility varies significantly between species (Douglas et al., 2000; Fuchikami et al., 2017).

Alternative *in vitro* methods to measure VSMC contractility include single-cell shortening (Ahmetaj-Shala et al., 2021), electric cell-substrate impedance sensing (Bogunovic et al., 2019) and traction force microscopy (Petit et al., 2021). In these methods, cells are isolated and assessed under conventional monolayer conditions, which fail to accurately reproduce interactions between VSMCs and the extracellular matrix—factors which are crucial in maintaining a mature and contractile phenotype (Swiatlowska et al., 2022). These issues are partially addressed with the 3D collagen gel contraction assay, which also is used to determine VSMC contractile phenotype (Jia et al., 2022; Wu et al., 2017) but is negated by difficulties in reliable quantification and reproducibility (Chen et al., 2013). Above all, the ability to measure VSMC contractility *in vitro* is severely undermined by the rapid and marked loss of contractility during culture, in favour of a more migratory and phagocytic phenotype (Chamley-Campbell et al., 1979; Proudfoot & Shanahan, 2012).

Advances in tissue engineering and materials science have enabled the development of three-dimensional vascular cell culture systems (Fleischer et al., 2020). In traditional, two-dimensional tissue culture, a combination of anticontractile factors in media supplements and the nonphysiological stiffness of tissue culture plastic, result in the dedifferentiation of VSMCs (Sandison et al., 2016; Swiatlowska et al., 2022), rendering them unsuitable for studying vascular contractility. Replication of the native mechanical environment

What is already known

- Pulmonary arterial hypertension is characterised by excessive, sustained contraction of vascular smooth muscle cells.
- Current laboratory methods fail to reliably reproduce the vasoactive behaviour of human pulmonary arteries.

What does this study add

- “Engineered pulmonary artery tissues” (EPATs) are miniature, three-dimensional contractile surrogates of human pulmonary arteries.
- The EPATs method is medium-throughput, cost-effective, technically straightforward, and accurately mimics human artery contractility.

What is the clinical significance

- EPATs are an innovative platform to conduct vasoactive drug screening for pulmonary arterial hypertension.
- This method will generate more effective treatments leading to reduced patient morbidity and mortality rates.

is essential for the maintenance of VSMC contractility (Swiatlowska et al., 2022) and, therefore, new cell culture platforms need to be established. Previously, miniaturised and spontaneously beating three-dimensional “engineered heart tissues” have been developed to measure contractility of primary and iPSC (induced pluripotent stem cell)-derived cardiomyocytes in a 24-well format (Breckwoldt et al., 2017; Hansen et al., 2010). These constructs are fabricated using a biocompatible fibrin hydrogel combined with isolated cardiomyocytes, which leads to the formation over time of coherently beating “tissues.” This culture platform provides a physiological system for preclinical disease modelling and drug development, which has recently been adapted for use in studies of skeletal muscle dystrophy (Maffioletti et al., 2018; Pinton et al., 2023) and VSMCs (Reed et al., 2022).

Based on our engineered VSMC tissue (EVT) platform (Reed et al., 2022), we have demonstrated its application for measuring VSMC contractility *in vitro* and adapted it for use with pulmonary artery-derived VSMCs. We have evaluated the suitability of EPATs for pharmacological drug testing, disease modelling of PAH, and provided proof-of-concept for the incorporation of endothelial cells. Overall, EPATs represent an exciting new tool with the potential to transform our approach to preclinical vascular research.

2 | METHODS

2.1 | Experimental design

EPATs were generated from human pulmonary artery VSMCs and human pulmonary artery endothelial cells (HPAECs) to evaluate their contractility. The methodology was optimised for robustness and reproducibility, in comparison to human isolated pulmonary artery vessels, to maximise the applicability of the findings to improve the understanding and treatment of PAH.

2.2 | Fabrication of PDMS racks

Moulds to produce custom-made PDMS racks were created using computer-aided design software (Autodesk Fusion) and 3D-printing with black resin (Formlabs RS-F2-GPBK-04). The resin moulds were rinsed in isopropanol and treated with trichloro(1H,1H,2H,2H-perfluorooctyl)silane (Sigma 448931) to minimise adhesion. PDMS racks of normal stiffness were produced by combining curing agent with the base reagent in a 1:10 ratio (VWR 634165S), mixing thoroughly with a plastic pasteur pipette and degassing for at least 2 h using a vacuum pump. Soft racks and stiff racks were made using a 1:15 ratio and 1:5 ratio of curing agent to base reagent, respectively. EHT (engineered heart tissue) racks, as used previously (Hansen et al., 2010), were purchased from a commercial source (EHT Technologies C0001). Next, PDMS was injected carefully into the mould, using a 10-ml syringe to avoid creating bubbles, then left to solidify at room temperature for at least 3 days before being removed from the moulds.

2.3 | Cell culture

Human pulmonary artery VSMCs were initially cultured in medium, containing supplements and penicillin–streptomycin (Gibco 15140-122; 100 U·ml⁻¹), in a humidified incubator at 37°C containing 5% CO₂. Cells were split in an approximately 1:3 ratio using trypsin/EDTA (Gibco 25300-062). All flasks and plates were coated with 0.2% gelatin (Sigma G1393) prior to cell seeding. Once cultures were established, cells were transferred to DMEM (Thermo Fisher 10313021) containing 10%–20% FBS (Gibco 10082-147; 20%), penicillin/streptomycin (Gibco 15140-122; 100 U·ml⁻¹), **L-glutamine** (Gibco 25030081; 200 mM), amphotericin B (Sigma A2942; 250 ng·ml⁻¹) and MycoZGAP (Lonza VZA-2031). Cells were used at passage 6–13 and donor information is listed in Table S1. HPAECs were obtained from commercial sources (detailed below) and cultured in a relevant endothelial cell medium, containing supplements and Pen/Strep (Gibco, 15140-122; 100 U·ml⁻¹), in a humidified incubator at 37°C containing 5% CO₂. All flasks and plates were coated with 10 µg·ml⁻¹ **fibronectin** (Sigma Aldrich, F1141) diluted in PBS (Sigma Aldrich D8537) prior to cell seeding. HPAECs were used at passage 9–13 and donor information is listed in Table S2.

2.4 | EPAT generation

EPATs were produced in a manner similar to previous reports which used cardiomyocytes, aortic smooth muscle cells and skeletal muscle myotubes (Breckwoldt et al., 2017; Pinton et al., 2023; Reed et al., 2022). Teflon spacers were boiled twice in dH₂O for 5 min each and autoclaved prior to use. PDMS racks were cleaned thoroughly with dH₂O and autoclaved prior to EPAT fabrication. After achieving at least 90% confluency and displaying a “hill and valley” morphology, VSMCs were considered suitable for EPAT fabrication. Per EPAT, a mastermix with 2.75-µl **fibrinogen** (Sigma F8630; 200 mg·ml⁻¹ in 0.9% NaCl), 101.2-µl DMEM (as used for culture) and 6.05 µl 2× DMEM (20% FBS, 100 U·ml⁻¹ penicillin–streptomycin in dH₂O) was prepared on ice. VSMCs were suspended in 110-µl mastermix per 1,100,000 cells. The cell mixture was triturated thoroughly before being cast. EPAT casting moulds were prepared by adding warm 2% agarose (Sigma A9539) in PBS into the wells of a 24-well plate (Thermo Fisher 144530) and placing Teflon spacers (EHT Technologies C0002) into these wells. Following the solidification of the agarose solution after 15 min, spacers were removed and the PDMS cell racks were placed into the wells such that every well contains a pair of posts. For each EPAT, 97 µl of mastermix containing VSMCs is added to 3-µl thrombin (Sigma T7513; 100 U·ml⁻¹ in PBS:H₂O [60:40]) and cast into the agarose wells. EPATs were then incubated at 37°C with 5% CO₂ for 90 min. Next, each of the wells was given 500-µl DMEM for 10 min to loosen each EPAT from the walls of the moulds. The EPATs were then transferred to a new 24-well plate with 1.5 ml EPAT medium (DMEM; 10% FBS; 100 U·ml⁻¹ penicillin–streptomycin; 200-mM L-glutamine; 0.1% **aprotinin** [Sigma A1153], 250 ng·ml⁻¹ amphotericin) per well. EPATs were maintained under standard culture conditions. The EPATs were subjected to a change of EPAT medium every Monday, Wednesday and Friday. For vasoreactivity experiments, EPATs had been fabricated at least 7 days prior.

2.5 | Vasoreactivity experiments

All EPAT vasoreactivity experiments were conducted using time-lapse widefield microscopy (Zeiss Axio Observer). The microscope was equipped with a temperature-controlled chamber and controlled by Zen acquisition software. To ensure sufficient pre-equilibration, all EPATs were incubated in serum-free DMEM (Thermo Fisher 21068028) containing 2.5-mM CaCl₂ under standard culture conditions for 3–4 h before any baseline reading measurements. All contractility measurements were performed using this medium. During baseline measurements, the EPATs were imaged every 5 min for a duration of 15 min, to verify the absence of contractility before adding vasoconstrictors. For the contraction and dilation experiments comparing EPATs of 500,000 versus 1,000,000 PASMCS, EPATs were exposed to KCl (75 mM) for 30 min to elicit contraction and then exposed to a combination of **nifedipine** (100 nM) and **sildenafil** (10 µM) for 30 min to elicit dilation; throughout, images were captured every 5 min. For vasoconstrictor concentration-response curves,

EPATs were exposed to increasing concentrations of vasoconstrictor (as stated) for 30 min each and images captured every 5 min. For vasodilator concentration-response curves, EPATs were first precontracted with **ET-1** (100 nM or 1 μ M) or **U46619** (1 μ M) for 1 h and images captured every 10 min, then EPATs were exposed to a given concentration of vasodilator (as stated) for 30 min each—in the presence of the same vasoconstrictor at the same concentration—and images captured every 5 min. These intervals were used as a compromise between the time required to image each EPAT individually (\sim 10 s per EPAT, up to 4 min for an entire plate [10s \times 24]) and the initial observed changes in contractile state (usually 5–10 min after exposure to drugs). Images were taken for longer periods (30–60 min) to ensure the maximum response to each drug was captured. Contractility experiments were performed at least 48 h apart to allow the EPATs to recover.

2.6 | Materials

Drugs were diluted to the desired working concentration in warm serum-free DMEM containing 2.5-mM CaCl_2 , vortexed thoroughly and then added to 24-well plates at 1.5 ml per well. Plates were incubated for at least 2 h prior to vasoreactivity experiments. Further information on sources of all vasoactive drugs used in this study are provided in Tables S3 and S4.

2.7 | Contractility data analysis

The distance between the PDMS posts is inversely proportional to the degree of contraction (Hansen et al., 2010). Images were exported into .tiff files using Zen Blue software and the precise distance between the posts was measured using the line function on FIJI. Data were exported to Microsoft Excel for further analysis. Data were first screened to exclude nonresponsive EPATs, deemed to be less than 5% maximum contraction (peak change in length). This threshold was employed following numerous observations that a contraction of less than 5% could not be sustained for more than 1 h and constitutes a very low signal-to-noise ratio, when accounting for technical issues such as image stitching and precise delineation of silicone posts. Baseline measurements of all other EPATs were then examined to ensure an adequate and complete equilibration to the baseline medium. Concentration-response curves and representative EPAT length traces were generated from the collected data using GraphPad Prism (Version 10). GraphPad Prism log (agonist/inhibitor) versus response (three parameter) nonlinear regression analysis was used to determine EC_{50} or IC_{50} values for vasoconstrictors or vasodilators. For vasoconstrictor concentration-response curves, the lowest stated concentration actually represents the change in length of EPATs between the first recorded image at baseline (0 min) and the last recorded image at baseline (15 min). Consistently, these changes were extremely minimal (<1%). For vasodilator concentration-response curves, the lowest stated concentration actually represents the maximal contraction

induced by the vasoconstrictor during the precontraction phase (without any vasodilator), with a mean value of 100%. This value was then used to calculate the amount of dilation, expressed as a percentage of the amount of maximum contraction. For example, an EPAT with the following measurements: baseline = 4 mm; precontraction with vasoconstrictor = 3 mm (25% contraction from baseline); vasoconstrictor plus vasodilator = 3.4 mm (15% contraction from baseline), results in a dilation of 40% ($100 - (15 \div 25 \times 100)$).

2.8 | Pulmonary artery VSMCs from PAH patients

Pulmonary artery VSMCs obtained from PAH patients were kindly provided by Professor Nick Morrell and Dr Paul Upton (University of Cambridge) and were isolated as previously described (Morrell et al., 1999). The demographics of these donors are listed in Table S5.

2.9 | Western blotting

The immuno-related procedures used comply with the recommendations made by the British Journal of Pharmacology (Alexander et al., 2018). Conditioned media were collected from EPATs, using a method adapted from a previous report (Yu et al., 2018). After 7 days following fabrication, EPATs were placed in warm PBS for 2 min, then transferred two times to serum-free, Phenol red-free DMEM (Thermo 31053028) containing Pen/Strep and glutamine (Thermo Fisher 10378016) for 30 min each and finally left for 24 h in a cell culture incubator. Conditioned media were collected on ice by pooling from 2–4 individual EPATs (3–6 ml in total), vortexed briefly and centrifuged at 500 g for 10 min to remove living cells, then 2000 g for 20 min to remove dead cells and finally for 5000 g for 15 min to remove cell debris. All centrifugation steps were performed at 4°C, samples were kept on ice in between spins and supernatant was transferred to new 15-ml Falcon tubes after each step. Equal volumes of sample were added into Amicon® 4 ml centrifugal filters (Merck UFC801024) and centrifuged at 5000 g (4°C) for 40 min, resulting in a \sim 50 \times concentration of media. Concentrated supernatant was transferred to low protein-binding 1.5 ml tubes (Sarstedt 72.703.600.) and stored at -80°C . For western blotting, samples were thawed on ice and centrifuged at 3000 g for 5 min at 4°C then diluted with 4 \times reducing Laemmli buffer (Alfa Aesar, J60015). Thereafter, samples were gently vortexed, boiled at 98°C for 5 min in a heating block, cooled on ice for 2 min and centrifuged at 16,000 g for 2 min. Equal sample volumes were loaded into 10-, 15- or 17-well NuPAGE 4%–12% Bis-Tris polyacrylamide gels (Thermo Fisher, NP0335BOX, NP0336BOX, NP0329BOX) alongside a broad-range protein standard (Thermo Fisher, 26634) and separated by electrophoresis at 100–200 V (Biorad, Powerpac 300) for 1–2 h using SDS running buffer (Invitrogen, NP0002-02), then washed briefly in H_2O and transferred to PVDF membranes (Biorad, 1704156) using the Transblot® Turbo™ transfer system (Biorad, 1704150). Next, membranes were washed in H_2O , blocked in milk

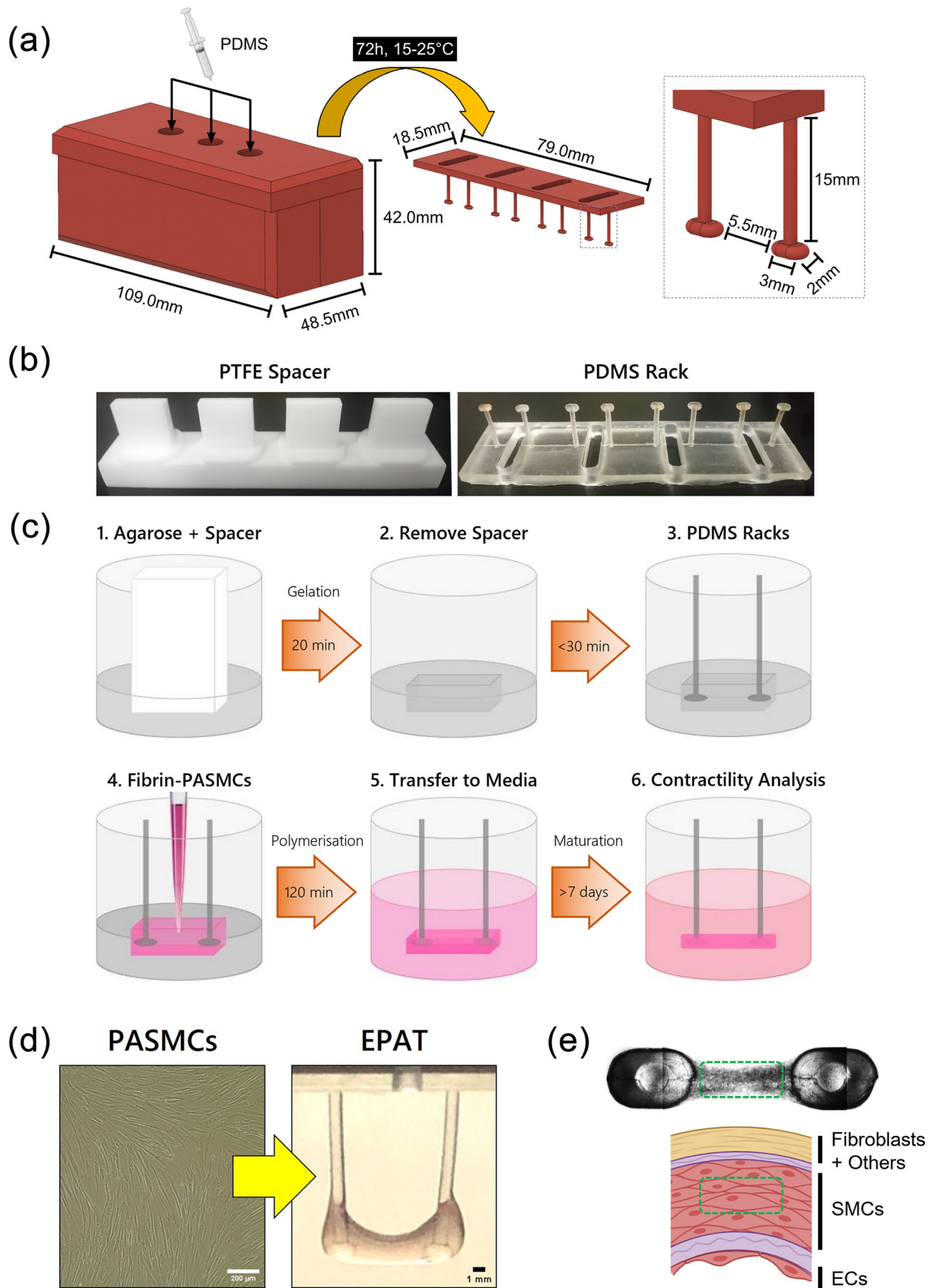


FIGURE 1 Legend on next page.

(EMD Millipore, 1.15363.0500; 5% in TBST) for 1 h and incubated at 4°C for a minimum of 16 h in primary antibody (PAI-1 (ab66705, rabbit polyclonal IgG, [RRID:AB_1310540](#); 1:1000); MMP-2 (Cell Signaling Technology 4022, rabbit polyclonal IgG, [RRID:AB_2266622](#); 1:1000)), diluted in 5% BSA (Sigma Aldrich, A9418) in TBST (Thermo Fisher, J77500). After, membranes were washed three times in TBST for 15 min each then incubated with HRP-conjugated secondary antibodies for anti-Rabbit (Sigma Aldrich A6154, goat polyclonal, [RRID:AB_258284](#); 1:2000) and anti-Mouse (Sigma Aldrich A6782, sheep polyclonal, [RRID:AB_258315](#); 1:2000) diluted in 5% BSA/TBST for 1 h followed by three washes in TBST for 10 min each. Imaging was performed using Immobilon® Forte HRP substrate (EMD Millipore, WBLUF0100) and a ChemiDoc system (Biorad, 731BR01754). To reprobe, membranes were washed twice in PBS for 2 min each, incubated with stripping buffer (Thermo Fisher, 21059) for 5–15 min, washed again in PBS before the protocol was repeated as above from the blocking step. Correct bands were identified by their molecular weight and quantified using the gel imaging tool on ImageJ. All values were normalised to MMP-2 as a loading control.

2.10 | Gelatin Zymography

Conditioned media were collected from EPATs as described above and gelatin zymography was performed as previously described (Yu et al., 2018). Polyacrylamide gels were produced containing 1 mg·ml⁻¹ gelatin (Sigma Aldrich G9391), Trizma base (Sigma Aldrich T1503; separating gel—375 mM, pH 8.8; stacking gel—125 mM, pH 6.8), acrylamide/bis-acrylamide (Sigma Aldrich A7802; separating gel—10%; stacking gel—4%), 0.1% SDS (Sigma Aldrich L3771), 0.1% ammonium persulfate (Sigma Aldrich A3678) and TEMED (Sigma Aldrich T9281; separating gel—1.25%; stacking gel—0.2%). Conditioned media samples were mixed with 2× nondenaturing sample buffer (125-mM Tris pH 6.8, 4% SDS, 20% glycerol, 50 µg·ml⁻¹ bromophenol blue) and separated by electrophoresis using zymography running buffer (240-mM Tris, 1.9-M glycine, 1% SDS) for 2 h at 120 V. Next, gels were washed briefly in water and incubated in 2.5% Triton X-100 for 30 min. Gels were then washed in incubation buffer (1% Triton X-100, 50-mM Tris, 5-mM CaCl₂, 1-µM ZnCl₂, 0.05% Na-Azide) for 5 min and then overnight in fresh incubation buffer at 37°C. Gels were then stained using Coomassie blue solution (40% MeOH, 10% acetic acid, 0.5-g Coomassie blue), washed thoroughly in water and destained in buffer (40% MeOH, 10% acetic acid) before imaging using the colorimetric setting on the

ChemiDoc system. Bands corresponding to the molecular weight of MMP-13 were quantified as described above using colour-inverted 8-bit images.

2.11 | Incorporation of endothelial cells

HPAECs (Promocell C-12241) were incorporated following a 3-day maturation period of the EPATs. EPATs casting moulds were prepared in a 24-well plate using the same protocol as described previously. Growth factor-reduced Matrigel (Corning 354230; 80 µg·ml⁻¹) was prepared and added to the moulds. The EPATs were placed in the moulds to be incubated with Matrigel for 5 min under standard culture conditions. The EPATs were removed from the moulds and transferred into empty wells on a 24-well plate for 2 min, allowing excess media to evaporate. The remaining Matrigel in the moulds was removed through aspiration. HPAECs were resuspended at a cell density of 1.5 × 10⁶ cells·ml⁻¹ with complete endothelial growth medium (Promocell C-22211); 80 µl of HPAECs suspension was added into each EPAT casting mould. The EPATs were returned to the moulds and were incubated for 60–120 min. During the incubation, the plate was inverted every 15–30 min to ensure an even incorporation of HPAECs around the EPAT. Brightfield images were captured during this process to confirm the attachment of HPAECs from the mould surface to the EPATs. The resulting EC-EPATs were maintained in complete endothelial growth medium supplemented with 33 µg·ml⁻¹ aprotinin. The EC-EPATs were allowed to mature for at least an additional 4 days prior to experiments. To maintain consistency, only one HPAEC donor was used and always paired with EPATs composed of HPA-VSMCs from Donor 6. Control EPATs containing only HPA-VSMCs were subjected to exactly the same protocol except that endothelial growth medium without HPAECs was added into the EPAT casting moulds.

2.12 | Fluorescence Microscopy

HPAECs were transfected with recombinant adenoviruses overexpressing GFP, 1 h prior to their incorporation into EPATs. Brightfield and fluorescent images were captured 2 weeks later using a Zeiss Axio Observer microscope at 472/30-nm excitation and 520/535-nm emission to observe GFP-expressing endothelial cells within EPATs. Z-stacks were captured to confirm the localisation of HPAECs specifically on the surface of EPATs, representing the endothelial monolayer present in blood vessels.

FIGURE 1 Experimental procedure for generating engineered pulmonary artery tissues (EPATs). (a) Protocol and schematic of computer-aided design images of the custom-made three-part resin mould (left) used to produce PDMS racks (centre) containing four pairs of posts (right) suitable for 24-well culture plates. (b) Photographs of commercially available PTFE (Teflon) spacer (left) and custom-made PDMS rack (right). (c) Protocol outline for fabricating EPATs from human pulmonary artery smooth muscle cells (PASMCS). (d) PASMCS in conventional monolayer culture (left) and a side-on image of a single EPAT (right). (e) Top-down image of a single EPAT taken using Widefield brightfield microscopy (top) alongside a schematic showing the cellular composition of the three layers of the vessel wall (bottom). The boxes with green dashed lines indicate that the PASMCS within EPATs represent the SMCs within the medial layer of the human pulmonary artery.

2.13 | Endothelium-dependent dilation

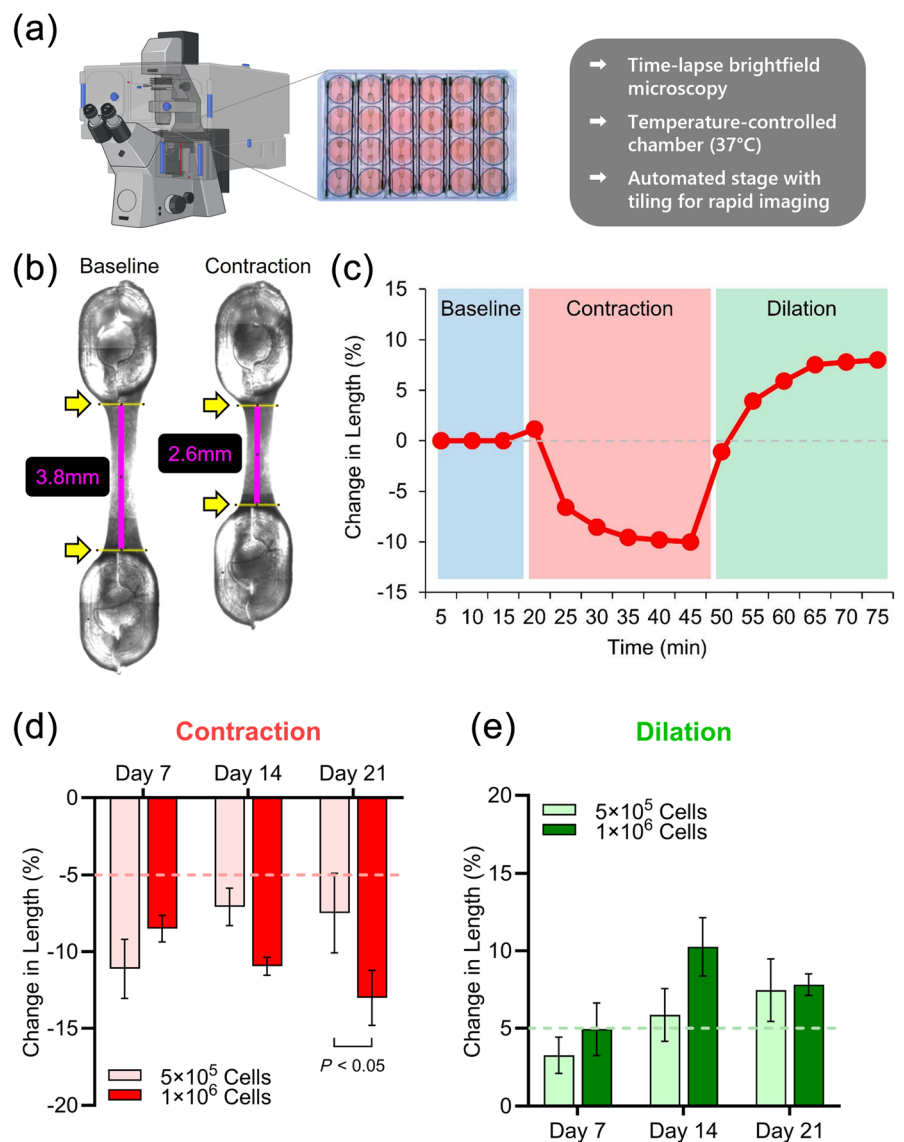
For dilation studies in EPATs containing HPAECs (EC-EPATs), experiments were performed as described in “Vasoreactivity Experiments,” wherein EC-EPATs (and controls) were equilibrated for 3–4 h, precontracted using U46619 (100 nM or 300 nM) for 1 h, then dilated using **carbachol** (100 μ M) for 30 min and then carbachol plus **histamine** (100 μ M or 300 μ M) for another 30 min. Carbachol and histamine were added in the presence of the same concentration of U46619 used to induce precontraction. All vasoreactivity experiments using EC-EPATs were performed in endothelial cell medium (without supplements) containing 0.1% FBS. EC-EPATs were only included in the final analyses if found to dilate >10% to either carbachol or the combination of carbachol and histamine. Images were captured every 5 min throughout the experiment, except for the precontraction phase of vasodilator studies where images were

captured every 10 min for a period of 1 h. For **ADMA** experiments, 300- μ M ADMA (Sigma D4268) was present in all solutions throughout, including during equilibration.

2.14 | Comparisons of EPATs with human pulmonary arteries

Published studies which evaluated the vasoactivity of healthy adult human pulmonary arteries (HPAs) were identified using the PubMed database. The vast majority of studies utilised the wire myography or organ bath technique. Data involving the same vasoactive compounds tested in EPATs (KCl, ET-1, U46619, **bosentan**, **epoprostenol/PGI₂**, **selexipag** / **MRE-269**, **imatinib**) were manually extracted in order to compare their efficacy and/or potency using the two different approaches. For the EPATs data, the mean and 95% symmetrical

FIGURE 2 Engineered pulmonary artery tissues (EPATs) exhibit robust contractility over time. (a) Microscope setup for performing contractility analysis of EPATs (adapted from Hansen et al., 2010). (b) Representative light microscopy images of the same EPAT before (left) and after (right) the addition of U46619 (1 μ M) for 30 min to induce contraction. Yellow arrows indicate length boundaries and purple lines represent EPAT, which are manually annotated for the quantitative analysis of EPAT contractility. (c) Representative trace showing the contraction and dilation of an EPAT as determined by the change in length. Contraction was induced by KCl (100 mM) and dilation by a combination of nifedipine (100 nM) and sildenafil (10 μ M). Bar charts showing (d) contraction of EPATs after 30 min of KCl (75 mM) and (e) dilation of EPATs after 30 min of a combination of nifedipine (100 nM) and sildenafil (10 μ M) containing two different amounts of PASMCs at day 7, 14 and 28 after fabrication ($n = 5-7$ from two donors in two independent experiments). P -values obtained from two-way ANOVA with Tukey's test.



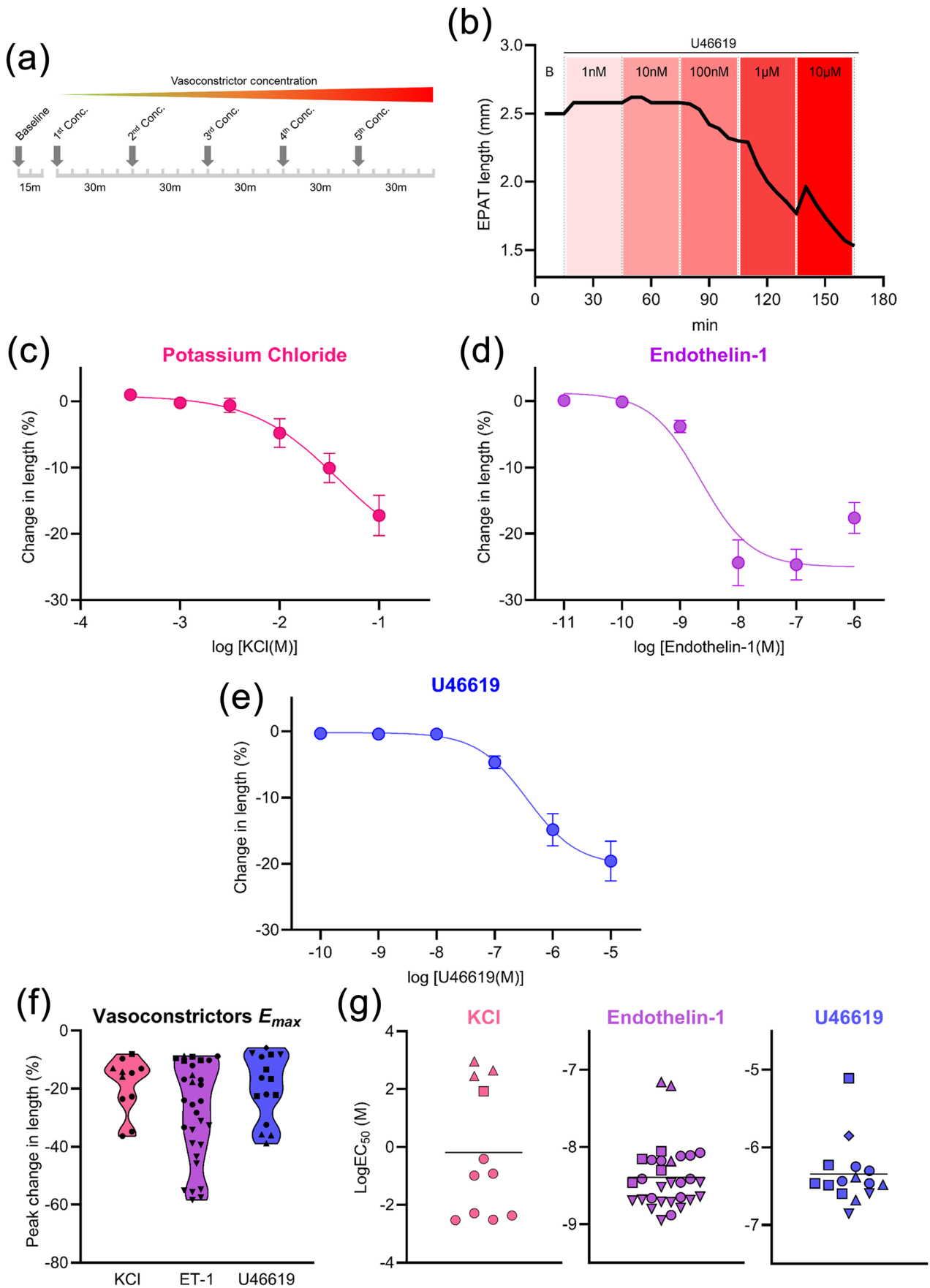


FIGURE 3 Legend on next page.

(asymptotic) confidence intervals were calculated directly from the non-linear regression curves (EC_{50}/IC_{50} values) or from the combined raw E_{max} values. From the HPA studies, data were compiled and presented as median [range] due to the low number of data points for certain groups. The raw data from each study are outlined and referenced in Tables S6 and S7.

2.15 | Data and statistical analysis

Recommendations were adhered to as set out in the *British Journal of Pharmacology* editorials for experimental design and analysis. Due to the method of fabrication and analysis, individual EPATs are treated as independent values rather than technical replicates. Equal group sizes were not possible due to inherent variability in VSMC growth in culture and occasional failure of EPATs during fabrication or analysis. All data subjected to statistical analysis contain at least $n = 5$ per group, although data with smaller sample sizes are included to demonstrate proof-of-concept. Samples were not randomised or blinded due to practical constraints during method development, but will be prioritised for future studies. Sigmoidal concentration–response curves were generated using nonlinear regression analysis of the \log_{10} concentration versus response (three parameters) to produce EC_{50}/IC_{50} values. Maximum responses (E_{max}) were defined as the value corresponding to the greatest response among technical replicates from the same biological donor in an individual experiment. P -values for differences between concentration–response curves were obtained from extra-sum-of-squares F test. Paired analyses were not performed because all comparisons were between groups, rather than the same samples over time. Statistical comparisons between three or more groups were performed with ordinary one-way or two-way ANOVA plus Tukey's multiple comparisons test. Gaussian distributions were confirmed using Shapiro–Wilk and Kolmogorov–Smirnov normality tests and equal variances were confirmed using Bartlett's and Browne–Forsythe's tests prior to further statistical analysis. Distributions and variances were only deemed to be different if all tests were $P < 0.01$. Variance between two groups was compared using an F test and statistical differences between two groups were performed using Student's t test. Data were presented as bar charts, violin plots or scatter plots. The threshold for statistical significance is defined as $P < 0.05$ throughout and is indicated as appropriate when comparing groups. Where appropriate, graphs are presented as mean \pm SEM (where $n \geq 3$) and mean \pm range (where $n = 2$). All analyses were conducted using GraphPad Prism 10.1.1. to 10.3.1.

2.16 | Nomenclature of targets and ligands

Key protein targets and ligands in this article are hyperlinked to corresponding entries in <https://www.guidetopharmacology.org> and are permanently archived in the Concise Guide to PHARMACOLOGY 2021/22 (Alexander et al., 2021).

3 | RESULTS

3.1 | Fabricating EPATs from human pulmonary artery VSMCs

The arterial extracellular matrix provides a greater stiffness on the resident cells compared with softer tissues such as the heart or skeletal muscle. Here, we formulated a method to produce racks for tissue constructs using 3D-printed resin moulds and polydimethylsiloxane (PDMS), a transparent, inert, nontoxic, flexible, gas-permeable polymer (Figure 1a), which were customisable in terms of stiffness. Teflon spacers and the custom-made PDMS racks (Figure 1b) were used to fabricate miniaturised, three-dimensional cellular constructs encapsulated in fibrin hydrogels between pairs of PDMS posts (Figure 1c). For the first time, we have used primary human pulmonary artery VSMCs (HPA-VSMCs) in this format to create EPATs (Figure 1d). Conceptually, EPATs represent the medial layer of the pulmonary artery wall which is composed of densely populated VSMCs (Figure 1e).

3.2 | EPATs as a novel platform for studying VSMC contractility

We developed a protocol to assess the contractile behaviour of EPATs as a surrogate marker of vasoreactivity. EPATs were assessed

TABLE 1 EC_{50} values for vasoconstrictors in EPATs compared with human pulmonary arteries (HPAs).

Method	Vasoconstrictor ($-\log EC_{50}$)		
	KCl	ET-1	U46619
EPATs	1.42 (0.88–1.95)	8.65 (8.31–8.99)	6.44 (6.03–6.86)
HPAs	1.54 [1.30–1.76]	8.29 [7.24–8.83]	7.70 [5.50–8.70]

Note: Values are given as mean (95% CI) for EPATs and median [range] for HPAs. The published data using HPAs are summarised in Table S6.

FIGURE 3 EPATs closely replicate human pulmonary artery responses to vasoconstrictors. (a) Experimental protocol for generating concentration-dependent responses with vasoconstrictors. (b) Representative line chart showing change in EPAT length over time in response to increasing concentrations of U46619. Concentration–response curves for the vasoconstrictors (c) KCl, (d) endothelin-1 and (e) U46619 generated within EPATs. (f) Violin plot showing maximal responses of each vasoconstrictor. Statistical comparisons were performed using one-way ANOVA with Tukey's test. (g) Scatter plots showing $\log EC_{50}$ values for each vasoconstrictor. Each symbol represents data obtained from an individual EPAT and each symbol shape represents a different PASM donor. KCl: $n = 11$ from three donors in three independent experiments, ET-1: $n = 30$ from four donors in six independent experiments, U46619: $n = 15$ from five donors in six independent experiments. P -values from one-way ANOVA with Tukey's test.

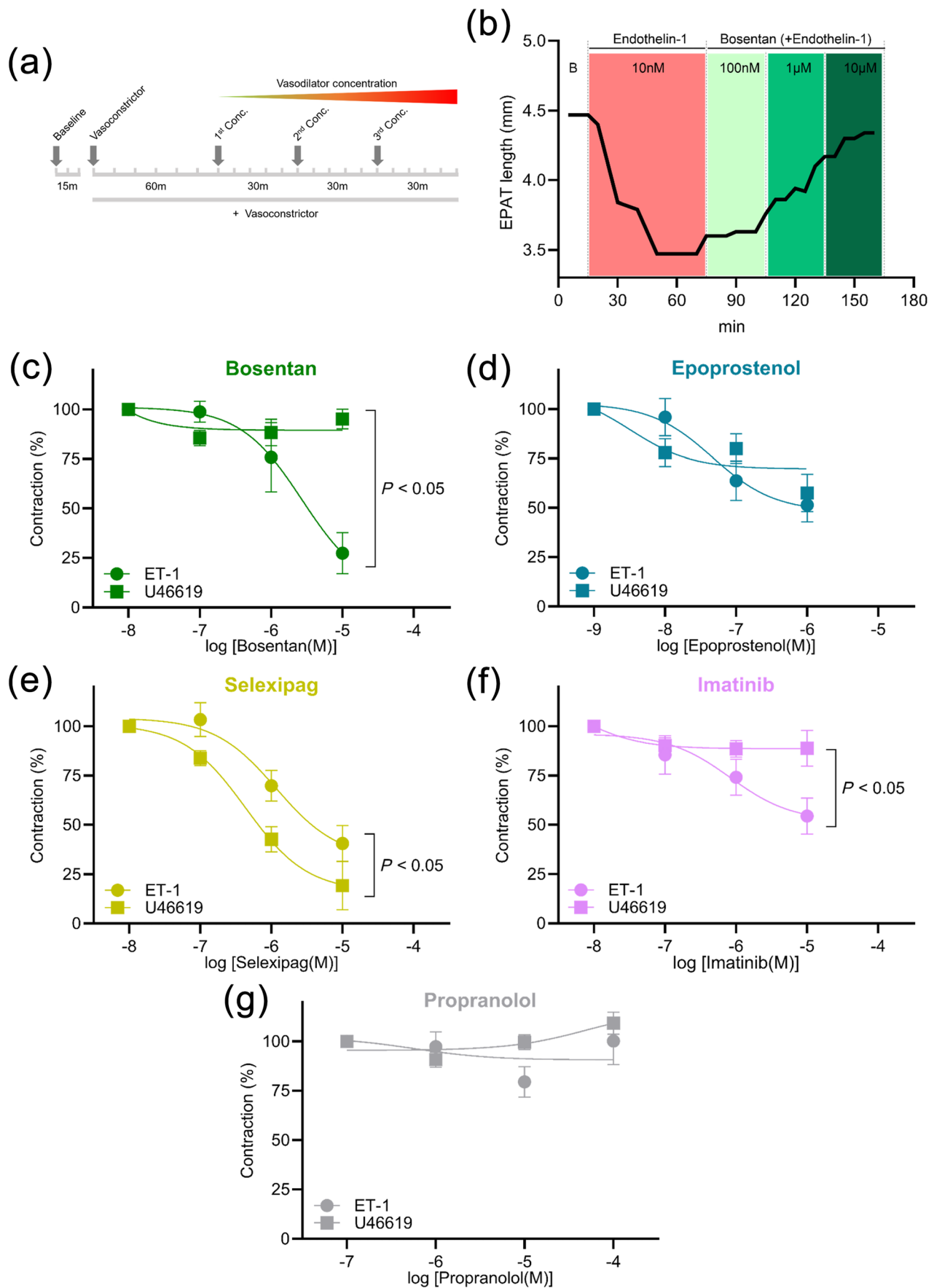


FIGURE 4 Legend on next page.

for contractility at weekly intervals, 7–21 days following tissue assembly, and analysis was conducted in 24-well plates and monitored by time-lapse brightfield microscopy inside a chamber maintained at 37°C (Figure 2a). Quantification of contractility was performed by analysis of images of individual EPATs (Figure 2b), where a reduction in length represents VSMC contraction (vasoconstriction) and an increase in length represents VSMC dilation (vasodilation). EPATs responded accordingly to vasoconstrictor and vasodilator agents, whereby maximal effect was reached within 10–15 min and maintained for 30 min after exposure (Figure 2c). The optimal number of cells required for the measurement of contractility was determined over time. At 7 days after fabrication, we observed a similar amount of contraction between EPATs containing 500,000 and 1,000,000 cells ($-11.1 \pm 1.9\%$ vs. $-8.5 \pm 0.9\%$). However, there was a greater degree of contraction within EPATs of 1,000,000 cells versus 500,000 cells at day 14 ($-10.9 \pm 0.6\%$ vs. $-7.1 \pm 1.2\%$) and day 21 ($-13.0 \pm 1.8\%$ vs. $-7.5 \pm 2.6\%$) (Figure 2d). Similar results were observed at day 14 when evaluating dilation (Figure 2e). PDMS racks for EPATs, which are customisable and cheaper compared with commercial racks, displayed greater levels of contraction (Figure S1). We also found that stiffer PDMS racks resulted in reduced contraction whereas softer racks produced greater contraction (Figure S2). In summary, EPATs composed of 1,000,000 VSMCs were best suited to contractile analysis over an extended time in culture. This also demonstrates a unique and powerful advantage of EPATs, to perform repeated contractility measurements over several weeks with no diminution in function.

3.3 | Pharmacological profiling of vasoconstrictors in EPATs

Next, we evaluated the ability of EPATs to produce concentration-dependent contractile responses and therefore generate vital data on drug pharmacology, as would be performed in myography studies (Figure 3a). EPATs showed a concentration-dependent contraction (Figure 3b) in response to three established vasoconstrictor drugs: potassium chloride (KCl) (Figure 3c), ET-1 (Figure 3d) and U46619 (Figure 3e). Crucially, the EC_{50} values and degrees of maximal contraction were almost identical to those observed in human pulmonary arteries (Dora et al., 2016) (Figure 3f,g; Table 1). We verified that concentration-dependent contraction and the level of maximal contraction were retained over several weeks (Figure S3). Additionally, individual EPATs were capable of robust and repeatable contractions to the same vasoconstrictor over time. Specifically, EPATs showed no

attenuation in contraction in response to U46619 in multiple experimental repeats over a 24-day period (Figure S3). Importantly, EPATs composed of VSMCs from different passage numbers exhibited similar levels of contraction and dilation (Figure S4). Also, EPATs containing VSMCs from the same biological donor at similar passage and time point, when exposed to the same concentration of ET-1 showed a highly similar degree of contraction when the entire experimental method is performed independently several months apart (Figure S4). Moreover, only approximately 5%–10% of EPATs failed to either assemble or contract sufficiently following fabrication. Altogether, this outlines the versatility, robustness, reproducibility and high success rate of the EPATs method.

3.4 | Pharmacological profiling of vasodilators in EPATs

We assessed concentration-dependent vasodilator responses in EPATs (Figure 4a). To do this, we induced EPAT contraction with a sub-maximal concentration of vasoconstrictor, which was gradually reversed by increasing concentrations of vasodilator (Figure 4b). Whereas the kinetics of EPATs contraction varied slightly according to VSMC donor, allowing maximal responses to develop over a 1-h period meant that stable contraction was achieved across all donors, prior to administration of vasodilators (Figure S5). In order to evaluate the potential suitability of EPATs as a platform for testing novel vasodilator therapies for PAH, we analysed various clinically available drugs in response to two PAH-relevant vasoconstrictors: ET-1 and U46619 (Weatherald et al., 2022; Wilson et al., 2018). With the endothelin receptor antagonist bosentan, EPATs displayed a near-complete reversal of contraction in the presence of ET-1 but were relatively unaffected when using U46619 (Figure 4c). Conversely, epoprostenol (prostacyclin) caused moderate levels of dilation to both ET-1 and U46619 (Figure 4d). The selective prostacyclin receptor agonist selexipag generated a strong reversal in contraction to both vasoconstrictors, with a greater effect in the presence of U46619 (Figure 4e). The tyrosine kinase inhibitor imatinib has demonstrated clinical efficacy in PAH patients but the underlying mechanism remains unknown (Wilkins et al., 2021). Interestingly, imatinib induced dilation in the presence of ET-1 but had no effect on U46619 (Figure 4f). To confirm that the observed responses were linked to vasodilatory actions of the tested drugs, we also assessed the effect of **propranolol**—a nonselective β -adrenoceptor antagonist used in the treatment of systemic hypertension. The antihypertensive impact of

FIGURE 4 EPATs reproduce vascular contractile responses to pulmonary arterial hypertension vasodilator therapies. (a) Experimental protocol for generating concentration-dependent responses with vasodilators following precontraction with either endothelin-1 (100 nM/1 μ M) or U46619 (1 μ M). (b) Representative line chart showing change in EPAT length over time in response to increasing concentrations of bosentan after precontraction with endothelin-1. Concentration–response curves for the vasodilators (c) bosentan, (d) epoprostenol, (e) selexipag, (f) imatinib plus and (g) propranolol, generated within EPATs. Bosentan: $n = 8$ from two donors in three independent experiments, epoprostenol: $n = 8$ from two donors in three independent experiments, selexipag: $n = 7$ –8 from two donors in three independent experiments, imatinib: $n = 11$ –14 from three to four donors in three to four independent experiments, propranolol: $n = 11$ –13 from two donors in four independent experiments. *P*-values obtained from extra-sum-of-squares *F* test.

propranolol is primarily due to blockade of cardiac β_1 -adrenoceptors, although studies in mouse pulmonary arteries show that smooth muscle β_2 -adrenoceptor stimulation elicits vasodilation (Leblais et al., 2008; Neumann et al., 2018), meaning that propranolol is not recommended for use in PAH in patients (Humbert et al., 2023). Accordingly, propranolol exerted no vasodilatory impact in EPATs (Figure 4g), although, at higher concentrations (100 μ M), propranolol induced a rapid and extreme increase in EPAT length (Figure S6), likely as a result of cytotoxicity, as reported previously in human lung cells (Kastelova et al., 2003). A summary comparison of maximal responses (E_{max}) revealed that selexipag was the only vasodilator that showed significantly greater levels of dilation versus propranolol, in the presence of both ET-1 and U46619 (Figure S7). Although considerable variation was observed in vasodilator potency (EC_{50}/IC_{50} values) for all vasodilators (except selexipag), significant differences between ET-1 and U46619 were found for bosentan and epoprostenol (Figure S7). Again, the EC_{50}/IC_{50} values and degree of maximal dilation of the four vasodilators were highly similar to those observed in human pulmonary arteries (Table 2). Overall, EPATs recapitulate the contractile behaviour and pharmacological profile of the human pulmonary artery in response to vasoactive drugs related to PAH.

3.5 | EPATs for PAH disease modelling

We then determined whether EPATs can model the excessive vasoconstriction observed in PAH, by fabricating EPATs using VSMCs obtained from the pulmonary arteries of PAH patients (Figure 5a). Remarkably, even in the absence of any vasoconstrictor stimuli, PAH EPATs exhibited spontaneous, progressive contraction over a period of several weeks in culture, whereas healthy EPATs showed little change over time (Figure 5b). Furthermore, we observed different concentration-response curves in PAH versus healthy EPATs in response to both ET-1 (Figure 5c) and U46619 (Figure 5d). PAH VSMCs displayed enhanced

contraction, predominantly in the presence of sub-maximal concentrations of vasoconstrictor. No differences were observed between healthy and PAH EPATs in terms of the degree of maximal contraction or vasoconstrictor EC_{50} values (Figure S8). We also repeated concentration-response curve experiments with the four vasodilators (bosentan, epoprostenol, selexipag, imatinib) in PAH EPATs (Figure 5e-h). Overall, the vasodilatory capacity of epoprostenol, selexipag and imatinib was enhanced in PAH EPATs compared with healthy EPATs, with epoprostenol and selexipag showing a particularly marked increase in maximal dilation and also, in some comparisons, differences in potency (Figures S9 and S10). We also stratified the PAH-EPATs according to whether the donors had idiopathic or heritable disease, which revealed significant differences in concentration-dependent contraction in response to U46619, but not to ET-1 (Figure S11). In addition to excessive vasoconstriction, the other primary clinical driver of PAH is vascular remodelling, characterised by hyperproliferation of VSMCs and substantial modifications to the surrounding extracellular matrix (Humbert, Sitbon, et al., 2023). Importantly, PAH EPATs recapitulated such pathophysiological changes following analysis of secreted proteins in the conditioned media. Compared with healthy controls, PAH EPATs showed reduced expression of plasminogen activator inhibitor-1 (PAI-1) as shown by western blotting as well as raised MMP-13 activity upon analysis by gelatin zymography (Figure S12). Both of these factors are predominantly expressed by VSMCs in the vascular wall and are known contributors to vascular remodelling in pulmonary hypertension (Herget et al., 2003; Kudryashova et al., 2024). In summary, EPATs are highly suited to measure a range of vascular disease responses related to PAH.

3.6 | Incorporation of HPAECs into EPATs

The endothelium plays a crucial role in the regulation of vascular contractility and in the pathophysiology and treatment of PAH (Humbert,

TABLE 2 EC_{50}/IC_{50} and E_{max} values for vasodilators in EPATs compared with human pulmonary arteries (HPAs).

Parameter	Method	Vasoconstrictor	Vasodilator			
			Bosentan	Epoprostenol	Selexipag	Imatinib
$-\log EC_{50}/IC_{50}$	EPATs	ET-1	5.56 (4.70–6.43)	7.33 (6.50–8.17)	5.93 (5.36–6.51)	6.08 (5.12–7.05)
		U46619	-	8.48 (6.99–9.98)	6.36 (5.89–6.84)	-
	HPAs	Various	6.00	7.08 [6.19–8.36]	6.19 [5.96–7.74]	5.42
E_{max} (% relaxation)	EPATs	ET-1	72.8 (48.4–97.1)	52.6 (33.6–71.7)	66.0 (46.3–85.7)	49.4 (29.8–69.1)
		U46619	21.3 (11.4–31.1)	32.5 (14.6–50.4)	83.2 (57.3–109.1)	19.7 (4.1–35.3)
	HPAs	Various	100.0	85.5 [60.0–100.0]	83.0 [69.0–97.0]	66.0

Note: Values are given as mean (95% CI) for EPATs and median [range] for HPAs. IC_{50} values for bosentan and imatinib in the presence of U46619 could not be calculated as their effect sizes were minimal. The published data using HPAs are summarised in Table S7.

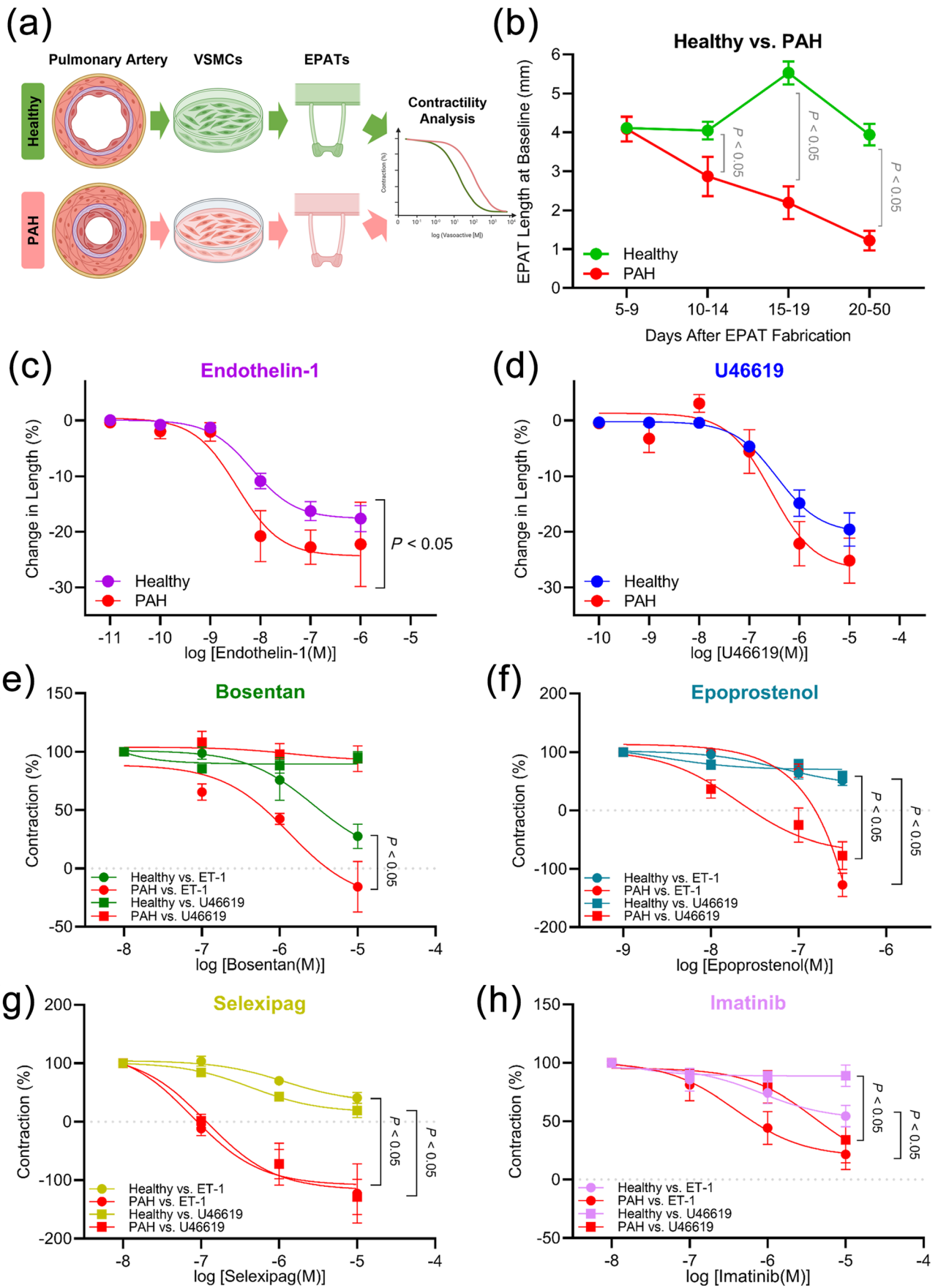


FIGURE 5 Legend on next page.

Sitbon, et al., 2023). Therefore, for future research it is highly advantageous to produce multi-cellular EPATs which are composed of pulmonary artery VSMCs with a monolayer of HPAECs to mimic arterial cell–cell interactions. Based on a previous report (Jin et al., 2020), we formulated a protocol to integrate HPAECs into EPATs using a basement membrane hydrogel (Matrigel) as a substrate (Figure 6a). The transfer of HPAECs into EPATs was evident by both brightfield imaging during fabrication (Figure S13) and in situ visualisation using fluorescence microscopy (Figure 6b, Figure S14). Crucially, following precontraction with U46619, EPATs containing HPAECs displayed rapid and potent dilation to a combination of carbachol and histamine, two endothelium-dependent vasodilators (Figure 6c). Dilation was achieved in the presence of HPAECs, whereas no response was noted for EPATs containing VSMCs alone (Figure 6d). Furthermore, endothelial dysfunction was induced using the endogenous **nitric oxide synthase** (NOS) inhibitor asymmetric dimethylarginine (ADMA), an established PAH driver and biomarker previously shown to be increased in the pulmonary endothelium during disease (Iannone et al., 2014; Pullamsetti et al., 2005). Accordingly, ADMA markedly reduced endothelium-dependent dilation to carbachol in EC-EPATs (Figure 6e). This shows that EC-EPATs are capable of mimicking endothelial dysfunction in vitro and therefore greatly increases the utility of EPATs as a PAH drug testing platform.

3.7 | Discussion and conclusions

Building on our EVT platform (Reed et al., 2022) we have adapted it for the measurement of vasoreactivity in vitro. EVTs and EPATs offer several advantages over currently used techniques, including three-dimensional orientation of VSMCs, exposure to passive mechanical stretch, physiological cell alignment and elongation. For the first time, we now demonstrate rapid and reproducible responses that replicate the contractile behaviour of small and medium pulmonary arteries. In addition, EPATs have several advantages over myography, the current gold standard method for measuring vascular contractility. These advantages include cost-effectiveness, technical simplicity, and easy accessibility of the required equipment and laboratory reagents. Importantly, EPATs are composed of human cells, eliminating the need for fresh tissue and carrying achievable implications for the replacement and reduction of animal use in such experiments.

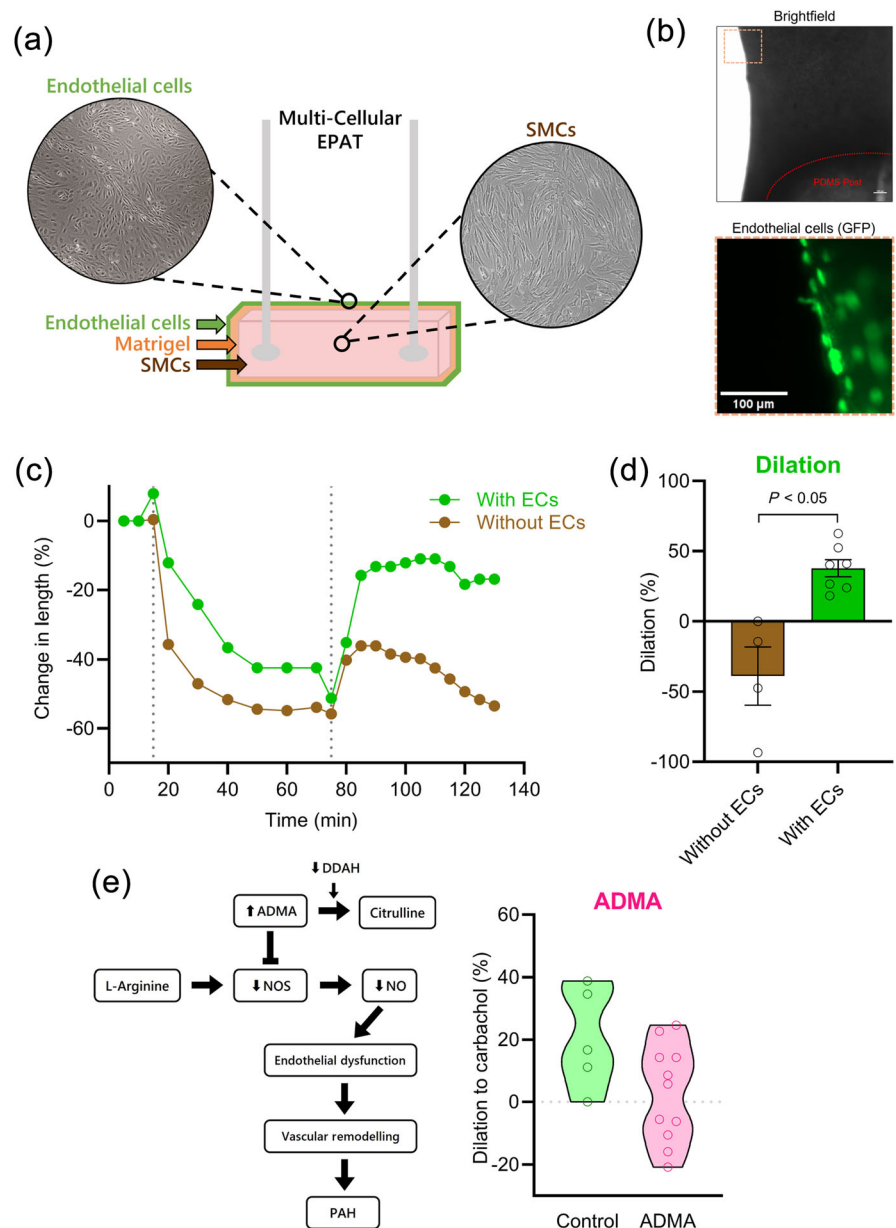
Another unique advantage of EPATs is that individual constructs remain contractile for at least 21 days after fabrication. Consequently, this enables a high volume of repeat testing and productivity and also the potential for more predictive, long-term preclinical modelling of PAH responses, analogous to those performed in animal studies.

Crucially, we have demonstrated that EPATs exhibit contractility which is highly similar to that observed in human pulmonary arteries. Using three different vasoconstrictors (KCl, ET-1, U46619), concentration–response curves revealed that EC_{50} values were extremely close to those found in previous studies using isolated human pulmonary arteries (Table 1; Table S6). In terms of efficacy, comparing the degree of maximal contraction was rarely possible due to variability in the reported units of measurement in other studies, for example, results from myography are often reported in terms of force/tension or as a percentage of maximum (usually in response to a high concentration of KCl). Nevertheless, we found that maximal contraction (E_{max}) for U46619 in EPATs was $-19.7 \pm 3.0\%$, which is comparable to the $26.0 \pm 5.0\%$ previously described in human pulmonary arteries (Dora et al., 2016). EPATs also were able to faithfully replicate the pharmacological profile of four vasodilators (bosentan, epoprostenol, selexipag and imatinib) (Table 2; Table S7), all of which are clinically effective treatments for PAH.

Given the established pathophysiological roles of both the **endothelin and thromboxane receptor** pathways in PAH (Clapp et al., 2020), we tested all vasodilators in the presence of both ET-1 and U46619. We found different vasodilatory responses between selexipag and epoprostenol, even though they are both agonists for the **prostacyclin receptor**. The differences we observed may be attributed to the fact that epoprostenol binds multiple other prostanoid receptors, whereas selexipag and its active metabolite are highly selective for the prostacyclin receptor (Douglas et al., 2000; Fuchikami et al., 2017). Epoprostenol also induces vasodilation via production of endothelial **NO** (Fuchikami et al., 2017). Clinically, epoprostenol is only recommended for PAH patients with advanced disease, who are already being treated with an endothelin receptor antagonist (e.g., bosentan or **macitentan**) and a nitric oxide modulator (e.g., sildenafil or **riociguat**) (Humbert, Sitbon, et al., 2023). In the future, it would be beneficial to determine how various PAH vasodilator therapies perform in combination as well as individually. Our observations of potential cytotoxicity with high concentrations of propranolol reveal another application of EPATs in preclinical testing

FIGURE 5 PAH-EPATs as a new tool for disease modelling and drug testing. (a) Experimental outline for the comparison of healthy and PAH EPATs. (b) Time course showing baseline length of EPATs made using PSMCs from healthy donors and PAH patients. Concentration–response curves of EPATs made using PSMCs from healthy donors and PAH patients in response to (c) endothelin-1, (d) U46619, (e) bosentan, (f) epoprostenol, (g) selexipag and (h) imatinib. Number of replicates for healthy EPATs as previously stated for Figures 3d,e and 4c–f. For PAH, ET-1: $n = 12$ from four donors in seven independent experiments; U46619: $n = 17$ from four donors in nine independent experiments; bosentan versus ET-1: $n = 12$ from four donors in three independent experiments; bosentan versus U46619: $n = 12$ from four donors in three independent experiments; epoprostenol versus ET-1: $n = 11$ from four donors in four independent experiments; epoprostenol versus U46619: $n = 9$ from three donors in three independent experiments; selexipag versus ET-1: $n = 5$ from two donors in one independent experiment; selexipag versus U46619: $n = 6$ from one donor in one independent experiment; imatinib versus ET-1: $n = 13$ from four donors in four independent experiments; imatinib versus U46619: $n = 10$ from four donors in four independent experiments. *P*-values obtained from multiple Mann–Whitney tests with FDR correction (b) and from extra-sum-of-squares *F* tests (c–h).

FIGURE 6 Incorporating human pulmonary artery endothelial cells into EPATs. (a) Schematic showing the protocol for incorporating endothelial cells into EPATs, by first coating the smooth muscle cells in Matrigel for 30 min, then adding endothelial cells to form a monolayer, as shown by expression of GFP. (b) Brightfield and fluorescent images showing the presence of human pulmonary artery endothelial cells (ECs) expressing GFP as a monolayer on the surface of EPATs. (c) Representative trace showing an EPAT with and without ECs, first contracting in response to U46619 (100 nM) and then dilating in response to a combination of carbachol (100 μ M) and histamine (100 μ M). (d) Bar chart showing the difference in dilation between EPATs with and without endothelial cells ($n = 4-7$ from one donor in three independent experiments). P -value obtained from unpaired two-tailed t -test. (e) Summary schematic showing the role of ADMA in PAH and violin plot showing dilation of EC-EPATs in response to carbachol (100 μ M) after 10 min ($n = 5-11$ from one donor [both cell types] in two independent experiments). P -value obtained from unpaired, two-tailed t -test.



regarding drug safety. Such approaches using engineered heart tissues have been previously employed (Saleem et al., 2020) and may serve to improve the efficiency of toxicity studies, by revealing parameters such as the toxic threshold concentration of a drug on the vasculature earlier on in the testing process.

We have discovered that PAH EPATs contracted more excessively compared with healthy EPATs in response to sub-maximal concentrations of ET-1. Recent studies have revealed that ET_A receptor expression remains unchanged in PAH (Hall et al., 2011; Wilson et al., 2018), which suggests an underlying heightened cellular sensitivity to ET-1 at the level of Ca^{2+} flux or the contractile apparatus. Our results also show strong evidence in favour of imatinib as a vasodilator. Previous studies in animal models have demonstrated the efficacy of imatinib in reversing pulmonary hypertension via inhibition of cell-growth related kinases and mitigation of vascular remodelling (Schermyly et al., 2005), supported by two-placebo controlled

randomised clinical trials (Ghofrani et al., 2010; Hoeper et al., 2013). Imatinib remains a viable PAH drug candidate, especially after reports suggesting it has an additional vasodilatory capacity (Abe et al., 2011; Pankey et al., 2013; Rieg et al., 2019). Our results in EPATs validate and confirm these findings and highlight the utility of EPATs for testing novel and emerging vasoactive drug candidates for PAH.

Low accessibility of PAH VSMCs may be a limiting factor in future applications of this platform for patient-specific responses to drugs, although generation of induced pluripotent stem cell-derived vascular smooth muscle and endothelial cell lines may offer a solution. Variability is particularly evident in the EC_{50}/IC_{50} values of certain vasodilators, and it is important to emphasise that such differences, as well as those seen between healthy and PAH EPATs may be due to several factors such as age and sex of donor, donor drug exposure and method of cell isolation. Whereas we have not fully characterised the pharmacology of endothelium-dependent responses in EPATs, we

successfully incorporated HPAECs into EPATs and demonstrated their functionality in dilation. This is a crucial step towards improving the physiological complexity of EPATs, which will be particularly valuable for the preclinical disease modelling and drug testing (Schermyly et al., 2011).

In summary, this study presents a low-cost, reproducible method of evaluating of human VSMC contractility, with multiple measurements performed over a prolonged period of time. We also have shown that EPATs can be applied to preclinical drug testing and disease modelling for cardiovascular disease.

AUTHOR CONTRIBUTIONS

A. L. Fellows: Conceptualization (lead); data curation (lead); formal analysis (lead); funding acquisition (lead); investigation (lead); methodology (lead); project administration (lead); resources (lead); software (lead); supervision (lead); validation (lead); visualization (lead); writing—original draft (lead); writing—review and editing (lead). **K. Quigley:** Data curation (supporting); investigation (supporting); validation (supporting). **V. Leung:** Data curation (supporting); investigation (supporting); validation (supporting). **A. J. Ainscough:** Methodology (supporting). **M. R. Wilkins:** Funding acquisition (supporting); supervision (supporting). **H. Barnett:** Methodology (supporting); resources (supporting). **D. Miller:** Methodology (supporting); resources (supporting). **M. Mayr:** Conceptualization (supporting). **B. Wojciak-Stothard:** Conceptualization (supporting); funding acquisition (supporting); project administration (supporting) resources (supporting); supervision (supporting); writing—original draft (supporting); writing—review and editing (supporting).

ACKNOWLEDGMENTS

We gratefully acknowledge the Facility for Imaging by Light Microscopy (FILM) at Imperial College London for their important contributions. We would like to thank Professor Nick Morrell, Dr Paul Upton and colleagues from the University of Cambridge for providing the VSMCs from PAH patients. We would also like to thank Professor Arne Hansen and colleagues at University Medical Center Hamburg-Eppendorf (UKE) for valuable advice, guidance and inspiration. This work was funded by the Imperial British Heart Foundation Centre of Research Excellence (AF) and an NHLI Foundation Pilot Award (AF). The Imperial College Advanced Hackspace is supported by HEIF (HB, DM).

CONFLICT OF INTEREST STATEMENT

The authors declare no conflicts of interest.

DATA AVAILABILITY STATEMENT

All raw data used in the study are available from the corresponding authors upon reasonable request.

DECLARATION OF TRANSPARENCY AND SCIENTIFIC RIGOUR

This Declaration acknowledges that this paper adheres to the principles for transparent reporting and scientific rigour of preclinical

research as stated in the *BJP* guidelines for [Natural Products Research](#), [Design and Analysis](#) and [Immunoblotting and Immunochemistry](#) and as recommended by funding agencies, publishers and other organisations engaged with supporting research.

ORCID

Adam L. Fellows  <https://orcid.org/0000-0002-9975-3795>

REFERENCES

- Abe, K., Toba, M., Alzoubi, A., Koubsky, K., Ito, M., Ota, H., Gairhe, S., Gerthoffer, W. T., Fagan, K. A., McMurtry, I. F., & Oka, M. (2011). Tyrosine kinase inhibitors are potent acute pulmonary vasodilators in rats. *American Journal of Respiratory Cell and Molecular Biology*, 45, 804–808. <https://doi.org/10.1165/rcmb.2010-0371OC>
- Ahmetaj-Shala, B., Marei, I., Kawai, R., Rothery, S., Pericleous, C., Mohamed, N. A., Gashaw, H., Bokea, K., Samuel, J., Vandenhede, A., Shala, F., Kirkby, N. S., & Mitchell, J. A. (2021). Activation and contraction of human “vascular” smooth muscle cells grown from circulating blood progenitors. *Frontiers in Cell and Development Biology*, 9, 681347. <https://doi.org/10.3389/fcell.2021.681347>
- Alexander, S. P. H., Roberts, R. E., Broughton, B. R. S., Sobey, C. G., George, C. H., Stanford, S. C., Cirino, G., Docherty, J. R., Giembycz, M. A., Hoyer, D., Insel, P. A., Izzo, A. A., Ji, Y., MacEwan, D. J., Mangum, J., Wonnacott, S., & Ahluwalia, A. (2018). Goals and practicalities of immunoblotting and immunohistochemistry: A guide for submission to the British Journal of Pharmacology. *British Journal of Pharmacology*, 175(3), 407–411. Portico. <https://doi.org/10.1111/bph.14112>
- Alexander, S. P., Kelly, E., Mathie, A., Peters, J. A., Veale, E. L., Armstrong, J. F., Faccenda, E., Harding, S. D., Pawson, A. J., Southan, C., Buneman, O. P., & Zolghadri, Y. (2021). The Concise Guide to PHARMACOLOGY 2021/22: Introduction and other protein targets. *British Journal of Pharmacology*, 178(Suppl 1), S1–S26. <https://doi.org/10.1111/bph.15537>
- Bogunovic, N., Meekel, J. P., Micha, D., Blankensteijn, J. D., Hordijk, P. L., & Yeung, K. K. (2019). Impaired smooth muscle cell contractility as a novel concept of abdominal aortic aneurysm pathophysiology. *Scientific Reports*, 9(1), 6837. <https://doi.org/10.1038/s41598-019-43322-3>
- Breckwoldt, K., Letuffe-Brenière, D., Mannhardt, I., Schulze, T., Ulmer, B., Werner, T., Benzin, A., Klampe, B., Reinsch, M. C., Laufer, S., Shibamiya, A., Prondzynski, M., Mearini, G., Schade, D., Fuchs, S., Neuber, C., Krämer, E., Saleem, U., Schulze, M. L., ... Hansen, A. (2017). Differentiation of cardiomyocytes and generation of human engineered heart tissue. *Nature Protocols*, 12, 1177–1197. <https://doi.org/10.1038/nprot.2017.033>
- Cahill, E., Rowan, S. C., Sands, M., Banahan, M., Ryan, D., Howell, K., & McLoughlin, P. (2012). The pathophysiological basis of chronic hypoxic pulmonary hypertension in the mouse: Vasoconstrictor and structural mechanisms contribute equally. *Experimental Physiology*, 97, 796–806. <https://doi.org/10.1113/expphysiol.2012.065474>
- Chamley-Campbell, J., Campbell, G. R., & Ross, R. (1979). The smooth muscle cell in culture. *Physiological Reviews*, 59, 1–61. <https://doi.org/10.1152/physrev.1979.59.1.1>
- Chen, H. C., Yang, T. H., Thoreson, A. R., Zhao, C., Amadio, P. C., Sun, Y. N., Su, F. C., & An, K. N. (2013). An automatic and quantitative measurement of collagen gel contraction using model-guided segmentation. *Measurement Science and Technology*, 24, 85702. <https://doi.org/10.1088/0957-0233/24/8/085702>
- Clapp, L. H., Abu-Hanna, J. H. J., & Patel, J. A. (2020). Diverse pharmacology of prostacyclin mimetics: Implications for pulmonary hypertension. In *Molecular mechanism of congenital heart disease and pulmonary hypertension*. Springer.

- Dora, K. A., Stanley, C. P., Al Jaaly, E., Fiorentino, F., Ascione, R., Reeves, B. C., & Angelini, G. D. (2016). Isolated human pulmonary artery structure and function pre- and post-cardiopulmonary bypass surgery. *Journal of the American Heart Association*, 5(2), e002822.
- Douglas, S. A., Sulpizio, A. C., Piercy, V., Sarau, H. M., Ames, R. S., Aiyar, N. V., Ohlstein, E. H., & Willette, R. N. (2000). Differential vasoconstrictor activity of human urotensin-II in vascular tissue isolated from the rat, mouse, dog, pig, marmoset and cynomolgus monkey. *British Journal of Pharmacology*, 131, 1262–1274. <https://doi.org/10.1038/sj.bjp.0703690>
- Fleischer, S., Tavakol, D. N., & Vunjak-Novakovic, G. (2020). From arteries to capillaries: Approaches to engineering human vasculature. *Advanced Functional Materials*, 30(37), 1910811. <https://doi.org/10.1002/adfm.201910811>
- Fuchikami, C., Murakami, K., Tajima, K., Homan, J., Kosugi, K., Kuramoto, K., Oka, M., & Kuwano, K. (2017). A comparison of vasodilation mode among selexipag (NS-304; [2-[4-[(5,6-diphenylpyrazin-2-yl)(isopropyl)amino]butoxy]-N-(methylsulfonyl)acetamide]), its active metabolite MRE-269 and various prostacyclin receptor agonists in rat, porcine and human pulmonary arteries. *European Journal of Pharmacology*, 795, 75–83. <https://doi.org/10.1016/j.ejphar.2016.11.057>
- Ghofrani, H. A., Morrell, N. W., Hoepfer, M. M., Olschewski, H., Peacock, A. J., Barst, R. J., Shapiro, S., Golpon, H., Toshner, M., Grimminger, F., & Pascoe, S. (2010). Imatinib in pulmonary arterial hypertension patients with inadequate response to established therapy. *American Journal of Respiratory and Critical Care Medicine*, 182, 1171–1177. <https://doi.org/10.1164/rccm.201001-0123OC>
- Hall, S. M., Davie, N., Klein, N., & Haworth, S. G. (2011). Endothelin receptor expression in idiopathic pulmonary arterial hypertension: Effect of bosentan and epoprostenol treatment. *The European Respiratory Journal*, 38, 851–860. <https://doi.org/10.1183/09031936.00167010>
- Hansen, A., Eder, A., Bönstrup, M., Flato, M., Mewe, M., Schaaf, S., Aksehirliglu, B., Schwoerer, A. P., Uebeler, J., & Eschenhagen, T. (2010). Development of a drug screening platform based on engineered heart tissue. *Circulation Research*, 107, 35–44. <https://doi.org/10.1161/CIRCRESAHA.109.211458>
- Herget, J., Novotná, J., Bíbová, J., Povýšilová, V., Vaňková, M., & Hampl, V. (2003). Metalloproteinase inhibition by Batimastat attenuates pulmonary hypertension in chronically hypoxic rats. *American Journal of Physiology-Lung Cellular and Molecular Physiology*, 285(1), L199–L208. <https://doi.org/10.1152/ajplung.00167.2002>
- Hoepfer, M. M., Barst, R. J., Bourge, R. C., Feldman, J., Frost, A. E., Galié, N., Gómez-Sánchez, M. A., Grimminger, F., Grünig, E., Hassoun, P. M., Morrell, N. W., Peacock, A. J., Satoh, T., Simonneau, G., Tapson, V. F., Torres, F., Lawrence, D., Quinn, D. A., & Ghofrani, H. A. (2013). Imatinib mesylate as add-on therapy for pulmonary arterial hypertension: Results of the randomized IMPRES study. *Circulation*, 127, 1128–1138. <https://doi.org/10.1161/CIRCULATIONAHA.112.000765>
- Humbert, M., Kovacs, G., Hoepfer, M. M., Badagliacca, R., Berger, R. M. F., Bida, M., Carlsen, J., Coats, A. J. S., Escribano-Subias, P., Ferrari, P., Ferreira, D. S., Ghofrani, H. A., Giannakoulas, G., Kiely, D. G., Mayer, E., Meszaros, G., Nagavci, B., Olsson, K. M., Pepke-Zaba, J., ... the ESC/ERS Scientific Document Group. (2023). 2022 ESC/ERS guidelines for the diagnosis and treatment of pulmonary hypertension. *The European Respiratory Journal*, 61, 2200879. <https://doi.org/10.1183/13993003.00879-2022>
- Humbert, M., Sitbon, O., Guignabert, C., Savale, L., Boucly, A., Gallant-Dewavrin, M., McLaughlin, V., Hoepfer, M. M., & Weatherald, J. (2023). Treatment of pulmonary arterial hypertension: Recent progress and a look to the future. *The Lancet Respiratory Medicine*, 11(9), 804–819. [https://doi.org/10.1016/S2213-2600\(23\)00264-3](https://doi.org/10.1016/S2213-2600(23)00264-3)
- Iannone, L., Zhao, L., Dubois, O., Duluc, L., Rhodes, C. J., Wharton, J., Wilkins, M. R., Leiper, J., & Wojciak-Stothard, B. (2014). miR-21/DDAH1 pathway regulates pulmonary vascular responses to hypoxia. *Biochemical Journal*, 462(1), 103–112. <https://doi.org/10.1042/bj20140486>
- Jia, Y., Mao, C., Ma, Z., Huang, J., Li, W., Ma, X., Zhang, S., Li, M., Yu, F., Sun, Y., Chen, J., Feng, J., Zhou, Y., Xu, Q., Zhao, L., Fu, Y., & Kong, W. (2022). PHB2 maintains the contractile phenotype of VSMCs by counteracting PKM2 splicing. *Circulation Research*, 131, 807–824. <https://doi.org/10.1161/CIRCRESAHA.122.321005>
- Jin, Q., Bhatta, A., Pagaduan, J. V., Chen, X., West-Foyle, H., Liu, J., Hou, A., Berkowitz, D., Kuo, S. C., Askin, F. B., Nguyen, T. D., Gracias, D. H., & Romer, L. H. (2020). Biomimetic human small muscular pulmonary arteries. *Science Advances*, 6(13), eaaz2598. <https://doi.org/10.1126/sciadv.aaz2598>
- Kastelova, A., Dimova, S., & Nemery, B. (2003). Propranolol cytotoxicity in rat and human lung in vitro. *Methods and Findings in Experimental and Clinical Pharmacology*, 25, 509–515. <https://doi.org/10.1358/mf.2003.25.7.778088>
- Kudryashova, T. V., Zaitsev, S. V., Jiang, L., Buckley, B. J., McGuckin, J. P., Goncharov, D., Zhyvlyo, I., Lin, D., Newcomb, G., Piper, B., Bogamuwa, S., Saiyed, A., Teos, L., Pena, A., Ranson, M., Greenland, J. R., Wolters, P. J., Kelso, M. J., Poncz, M., ... Stepanova, V. (2024). PAI-1 deficiency drives pulmonary vascular smooth muscle remodeling and pulmonary hypertension. *American Journal of Physiology-Lung Cellular and Molecular Physiology*, 327(3), L319–L326. <https://doi.org/10.1152/ajplung.00110.2024>
- Leblais, V., Delannoy, E., Fresquet, F., Bégueret, H., Bellance, N., Banquet, S., Allières, C., Leroux, L., Desgranges, C., Gadeau, A., & Muller, B. (2008). β -adrenergic relaxation in pulmonary arteries: Preservation of the endothelial nitric oxide-dependent β 2 component in pulmonary hypertension. *Cardiovascular Research*, 77, 202–210. <https://doi.org/10.1093/cvr/cvm008>
- Maffioletti, S. M., Sarcar, S., Henderson, A. B. H., Mannhardt, I., Pinton, L., Moyle, L. A., Steele-Stallard, H., Cappellari, O., Wells, K. E., Ferrari, G., Mitchell, J. S., Tyzack, G. E., Kotiadis, V. N., Khedr, M., Ragazzi, M., Wang, W., Duchon, M. R., Patani, R., Zammit, P. S., ... Tedesco, F. S. (2018). Three-dimensional human iPSC-derived artificial skeletal muscles model muscular dystrophies and enable multilineage tissue engineering. *Cell Reports*, 23, 899–908. <https://doi.org/10.1016/j.celrep.2018.03.091>
- Morrell, N. W., Upton, P. D., Kotecha, S., Huntley, A., Yacoub, M. H., Polak, J. M., & Wharton, J. (1999). Angiotensin II activates MAPK and stimulates growth of human pulmonary artery smooth muscle via AT 1 receptors. *The American Journal of Physiology*, 277, L440–L448. <https://doi.org/10.1152/ajplung.1999.277.3.L440>
- Neumann, V., Knies, R., Seidinger, A., Simon, A., Lorenz, K., Matthey, M., Breuer, J., & Wenzel, D. (2018). The β 2 agonist terbutaline specifically decreases pulmonary arterial pressure under normoxia and hypoxia via α adrenoceptor antagonism. *The FASEB Journal*, 32, 2519–2530. <https://doi.org/10.1096/fj.201700684RR>
- Pankey, E. A., Thammasitboon, S., Lasker, G. F., Baber, S., Lasky, J. A., & Kadowitz, P. J. (2013). Imatinib attenuates monocrotaline pulmonary hypertension and has potent vasodilator activity in pulmonary and systemic vascular beds in the rat. *American Journal of Physiology. Heart and Circulatory Physiology*, 305, 1288–1296. <https://doi.org/10.1152/ajpheart.00329.2013>
- Petit, C., Karkhaneh Yousefi, A. A., Ben, M. O., Michel, J. B., Guignandon, A., & Avril, S. (2021). Regulation of SMC traction forces in human aortic thoracic aneurysms. *Biomechanics and Modeling in Mechanobiology*, 20, 717–731. <https://doi.org/10.1007/s10237-020-01412-6>
- Pinton, L., Khedr, M., Lionello, V. M., Sarcar, S., Maffioletti, S. M., Dastidar, S., Negroni, E., Choi, S. W., Khokhar, N., Bigot, A., Counsell, J. R., Bernardo, A. S., Zammit, P. S., & Tedesco, F. S. (2023). 3D human induced pluripotent stem cell-derived bioengineered skeletal muscles for tissue, disease and therapy modeling. *Nature Protocols*, 18, 1337–1376. <https://doi.org/10.1038/s41596-022-00790-8>

- Proudfoot, D., & Shanahan, C. (2012). Human vascular smooth muscle cell culture. *Methods in Molecular Biology*, 806, 251–263. https://doi.org/10.1007/978-1-61779-367-7_17
- Pullamsetti, S., Kiss, L., Ghofrani, H. A., Voswinckel, R., Haredza, P., Klepetko, W., Aigner, C., Fink, L., Muyal, J. P., Weissmann, N., Grimminger, F., Seeger, W., & Schermuly, R. T. (2005). Increased levels and reduced catabolism of asymmetric and symmetric dimethylarginines in pulmonary hypertension. *The FASEB Journal*, 19(9), 1175–1177. Portico. <https://doi.org/10.1096/fj.04-3223fje>
- Reed, E., Fellows, A., Lu, R., Rienks, M., Schmidt, L., Yin, X., Duregotti, E., Brandt, M., Krasemann, S., Hartmann, K., Barallobre-Barreiro, J., Addison, O., Cuello, F., Hansen, A., & Mayr, M. (2022). Extracellular matrix profiling and disease modelling in engineered vascular smooth muscle cell tissues. *Matrix Biology Plus*, 16, 100122. <https://doi.org/10.1016/j.mbplus.2022.100122>
- Rieg, A. D., Bunting, N. A., Cranen, C., Suleiman, S., Spillner, J. W., Schnöring, H., Schröder, T., von Stillfried, S., Braunschweig, T., Manley, P. W., Schälte, G., Rossaint, R., Uhlig, S., & Martin, C. (2019). Tyrosine kinase inhibitors relax pulmonary arteries in human and murine precision-cut lung slices. *Respiratory Research*, 20, 111. <https://doi.org/10.1186/s12931-019-1074-2>
- Saleem, U., van Meer, B. J., Katili, P. A., Mohd Yusof, N. A. N., Mannhardt, I., Garcia, A. K., Tertoolen, L., de Korte, T., Vlaming, M. L. H., McGlynn, K., Nebel, J., Bahinski, A., Harris, K., Rossman, E., Xu, X., Burton, F. L., Smith, G. L., Clements, P., Mummery, C. L., ... Denning, C. (2020). Blinded, multicenter evaluation of drug-induced changes in contractility using human-induced pluripotent stem cell-derived cardiomyocytes. *Toxicological Sciences*, 176, 103–123. <https://doi.org/10.1093/toxsci/kfaa058>
- Sandison, M. E., Dempster, J., & McCarron, J. G. (2016). The transition of smooth muscle cells from a contractile to a migratory, phagocytic phenotype: Direct demonstration of phenotypic modulation. *The Journal of Physiology*, 594, 6189–6209. <https://doi.org/10.1113/JP272729>
- Schermuly, R. T., Dony, E., Ghofrani, H. A., Pullamsetti, S., Savai, R., Roth, M., Sydykov, A., Lai, Y. J., Weissmann, N., Seeger, W., & Grimminger, F. (2005). Reversal of experimental pulmonary hypertension by PDGF inhibition. *The Journal of Clinical Investigation*, 115, 2811–2821. <https://doi.org/10.1172/JCI24838>
- Schermuly, R. T., Ghofrani, H. A., Wilkins, M. R., & Grimminger, F. (2011). Mechanisms of disease: Pulmonary arterial hypertension. *Nature Reviews. Cardiology*, 8(8), 443–455. <https://doi.org/10.1038/nrcardio.2011.87>
- Stenmark, K. R., Meyrick, B., Galie, N., Mooi, W. J., & Mcmurtry, I. F. (2009). Animal models of pulmonary arterial hypertension: The hope for etiological discovery and pharmacological cure. *American Journal of Physiology. Lung Cellular and Molecular Physiology*, 297, 1013–1032.
- Swiatlowska, P., Sit, B., Feng, Z., Marhuenda, E., Xanthis, I., Zingaro, S., Ward, M., Zhou, X., Xiao, Q., Shanahan, C., Jones, G. E., Yu, C. H., & Iskratsch, T. (2022). Pressure and stiffness sensing together regulate vascular smooth muscle cell phenotype switching. *Science Advances*, 8(15), eabm3471.
- Weatherald, J., Boucly, A., Peters, A., Montani, D., Prasad, K., Psotka, M. A., Zannad, F., Gombert-Maitland, M., McLaughlin, V., Simonneau, G., Humbert, M., & Evolving Landscape of Pulmonary Arterial Hypertension and Redesigning Pulmonary Arterial Hypertension Clinical Trials Task Force of the 18th Global Cardiovascular Clinical Trialists Forum. (2022). The evolving landscape of pulmonary arterial hypertension clinical trials. *Lancet*, 400, 1884–1898. [https://doi.org/10.1016/S0140-6736\(22\)01601-4](https://doi.org/10.1016/S0140-6736(22)01601-4)
- Wenceslau, C. F., McCarthy, C. G., Earley, S., England, S. K., Filosa, J. A., Goulopoulou, S., Gutterman, D. D., Isakson, B. E., Kanagy, N. L., Martinez-Lemus, L. A., Sonkusare, S. K., Thakore, P., Trask, A. J., Watts, S. W., & Webb, R. C. (2021). Guidelines for the measurement of vascular function and structure in isolated arteries and veins. *American Journal of Physiology. Heart and Circulatory Physiology*, 321, H77–H111. <https://doi.org/10.1152/ajpheart.01021.2020>
- Wilkins, M. R., Mckie, M. A., Law, M., Roussakis, A. A., Harbaum, L., Church, C., Coghlan, J. G., Condliffe, R., Howard, L. S., Kiely, D. G., Lordan, J., Rothman, A., Suntharalingam, J., Toshner, M., Wort, S. J., & Villar, S. S. (2021). Positioning imatinib for pulmonary arterial hypertension: A phase I/II design comprising dose finding and single-arm efficacy. *Pulmonary Circulation*, 11(4), 20458940211052823. <https://doi.org/10.1177/20458940211052823>
- Wilson, J. L., Warburton, R., Taylor, L., Toksoz, D., Hill, N., & Polgar, P. (2018). Unraveling endothelin-1 induced hypercontractility of human pulmonary artery smooth muscle cells from patients with pulmonary arterial hypertension. *PLoS ONE*, 13, e0195780. <https://doi.org/10.1371/journal.pone.0195780>
- Wu, D., Ren, P., Zheng, Y., Zhang, L., Xu, G., Xie, W., Lloyd, E. E., Zhang, S., Zhang, Q., Curci, J. A., Coselli, J. S., Milewicz, D. M., Shen, Y. H., & LeMaire, S. A. (2017). NLRP3 (nucleotide oligomerization domain-like receptor family, pyrin domain containing 3)-caspase-1 inflammasome degrades contractile proteins implications for aortic biomechanical dysfunction and aneurysm and dissection formation. *Arteriosclerosis, Thrombosis, and Vascular Biology*, 37, 694–706. <https://doi.org/10.1161/ATVBAHA.116.307648>
- Yu, H., Fellows, A., Foote, K., Yang, Z., Figg, N., Littlewood, T., & Bennett, M. (2018). FOXO3a (forkhead transcription factor O subfamily member 3a) links vascular smooth muscle cell apoptosis, matrix breakdown, atherosclerosis, and vascular remodeling through a novel pathway involving MMP13 (matrix metalloproteinase 13). *Arteriosclerosis, Thrombosis, and Vascular Biology*, 38, 555–565. <https://doi.org/10.1161/ATVBAHA.117.310502>

SUPPORTING INFORMATION

Additional supporting information can be found online in the Supporting Information section at the end of this article.

How to cite this article: Fellows, A. L., Quigley, K., Leung, V., Ainscough, A. J., Wilkins, M. R., Barnett, H., Miller, D., Mayr, M., & Wojciak-Stothard, B. (2025). Engineered pulmonary artery tissues for measuring contractility, drug testing and disease modelling. *British Journal of Pharmacology*, 182(12), 2585–2602. <https://doi.org/10.1111/bph.17462>